Electromagnetic Energy Memory (EEM): A Resonant and Network-Based Framework for Non-Chemical Energy Storage

Mohamed Orhan Zeinel
Independent Researcher
mohamedorhanzeinel@gmail.com
ORCID: 0009-0008-1139-8102

November 13, 2025

DOI: 10.5281/zenodo.17597289

Abstract

Conventional electric energy storage is dominated by electrochemical devices such as batteries and supercapacitors. While highly successful, their performance is fundamentally constrained by material availability, degradation mechanisms, and safety limitations. This paper proposes *Electromagnetic Energy Memory* (EEM): a conceptual and mathematical framework in which energy is stored in purely electromagnetic and resonant structures, without chemical reactions. We consider a ring of resistive–inductive–capacitive (RLC) cells with capacitive coupling between neighbours, and we show that this network can support long-lived, spatially localized energy patterns. These patterns are interpreted as *energy memory states*. We derive the governing equations, define a rigorous notion of energy-level encoding, develop a modal analysis for the underlying RLC lattice, and present high-resolution numerical simulations demonstrating the emergence and persistence of localized modes under realistic loss. The results suggest that resonant LC networks can form the basis for a new class of non-chemical energy storage and signal-processing devices, complementing and potentially extending traditional electrochemical technologies.

Keywords: energy storage, LC networks, resonant systems, electromagnetic memory, localization, non-chemical batteries, circuit lattices.

1 Introduction

Electric energy storage is a core enabling technology for modern power systems, mobile electronics, and renewable integration. Today, this role is fulfilled almost exclusively by *electrochemical* devices, whose operation is based on reversible redox reactions and ionic transport. Despite decades of progress, electrochemical storage faces structural limitations: finite cycle life, complex thermal management, safety risks, and dependence on critical materials [1, 2, 3].

In parallel, the electromagnetic theory of circuits provides a different, purely field-based picture of energy. Even a simple ideal LC resonator can store energy indefinitely in alternating electric

and magnetic form. In practice, resistance and radiation losses cause decay, but carefully designed resonant networks can still exhibit long-lived modes and rich spatial structure.

This observation motivates a simple but fundamental question:

> *Can electric energy be stored and manipulated as a memory state in a purely electromagnetic network, without relying on chemical energy?*

In this paper we take a first step toward answering this question by introducing *Electromagnetic Energy Memory* (EEM). We focus on a linear, time-invariant circuit model—a ring of coupled LC cells with series resistance—and investigate whether it supports:

(i) spatially localized energy patterns;
(ii) persistence of such patterns over timescales much longer than the oscillation period;
(iii) robustness of these patterns to parameter changes and dissipation.

We interpret persistent localized patterns as *energy memory states* of the network.

The contributions of this work are:

- a clear mathematical formulation of EEM in terms of an RLC ring with capacitive coupling;
- a definition of energy-level encoding and electromagnetic memory states in networked resonant systems;
- a modal and dispersion analysis for the underlying circuit lattice;
- a high-precision numerical study demonstrating emergent energy localization and long-lived memory modes under realistic losses;
- a first quantitative discussion of energetic limits, efficiency, and the position of EEM within the broader energy-storage landscape.

This paper is intentionally exploratory. We do not claim immediate practical superiority over electrochemical storage. Instead, we aim to open a rigorous research direction for non-chemical, resonant energy storage and computation.

2 Background and Related Work

Resonant electrical networks and transmission-line analogues have long been used in filters, delay lines, and metamaterials [6, 7]. Lattice models with inductive and capacitive coupling are a standard tool in the study of wave propagation, dispersion, and localization in discrete systems [8].

Energy localization in nonlinear and disordered lattices is an established phenomenon, often discussed under the umbrella of *discrete breathers* and intrinsic localized modes [9, 10]. Electrical implementations of such lattices have been explored using nonlinear elements and PT-symmetric configurations [11].

In parallel, the search for alternatives to chemical energy storage has produced a range of physical concepts, including mechanical flywheels, superconducting magnetic energy storage (SMES), and compressed air systems [2, 4, 5]. Supercapacitors offer high power density and cycle life, but limited energy density, while SMES devices achieve exceptional cycle performance at the cost of cryogenic complexity and infrastructure.

To our knowledge, however, there is relatively little work that treats energy storage itself as a *distributed electromagnetic memory problem* in linear, passive circuit lattices.

EEM can be viewed as a bridge between these lines of research: it adopts the mathematical language of circuit lattices and localization, but uses it to formulate an explicit memory and storage paradigm, rather than focusing solely on wave propagation or nonlinearity.

3 Model: LC Ring with Capacitive Coupling

3.1 Circuit structure

We consider a one-dimensional ring of N identical cells. Each cell $k \in \{0, \dots, N-1\}$ contains:

- an inductance $L > 0$,
- a capacitance $C > 0$,
- a series resistance $R \geq 0$.

Cells are coupled to their nearest neighbours via a coupling capacitance $C_c > 0$. We enforce periodic boundary conditions:

$$q_{-1} = q_{N-1}, \qquad q_N = q_0, \tag{1}$$

where q_k denotes the charge on the capacitor of cell k.

3.2 State variables and equations of motion

For each cell k, let:

- $q_k(t)$ be the charge on the cell capacitor,
- $i_k(t) = \frac{q_k}{t}$ be the current through the inductor.

Neglecting radiation and assuming linear components, the dynamics follow from Kirchhoff's laws. The voltage across capacitor k is $V_k = q_k/C$. The coupling term penalizes differences in neighbouring charges.

The equation of motion for cell k is

$$L\frac{^2q_k}{t^2} + R\frac{q_k}{t} + \frac{1}{C}q_k + \frac{1}{C_c}\big(2q_k - q_{k-1} - q_{k+1}\big) = 0. \tag{2}$$

Introducing $i_k = \frac{q_k}{t}$, we obtain the first-order system

$$\frac{q_k}{t} = i_k, \tag{3}$$

$$\frac{i_k}{t} = -\frac{R}{L}i_k - \frac{1}{LC}q_k - \frac{1}{LC_c}\big(2q_k - q_{k-1} - q_{k+1}\big). \tag{4}$$

Collecting all cell variables into the state vector

$$\mathbf{y}(t) = \big(q_0, \dots, q_{N-1},\, i_0, \dots, i_{N-1}\big)^\top \in^{2N}, \tag{5}$$

we can write

$$\frac{\mathbf{y}}{t} = \mathbf{f}(\mathbf{y}), \tag{6}$$

with $\mathbf{f}$ defined by (3)–(4). In this paper we solve these equations numerically using a high-accuracy Runge–Kutta scheme.

3.3 Dimensionless formulation

For analytical convenience we introduce dimensionless variables. Let

$$\omega_0 = \frac{1}{\sqrt{LC}}, \qquad t' = \omega_0 t, \tag{7}$$

and define dimensionless parameters

$$\gamma = \frac{R}{L\omega_0}, \qquad \kappa = \frac{C}{C_c}. \tag{8}$$

Dropping primes, the second-order equation (2) becomes

$$\frac{^2q_k}{t^2} + \gamma\frac{q_k}{t} + q_k + \kappa\big(2q_k - q_{k-1} - q_{k+1}\big) = 0, \tag{9}$$

with all times measured in units of the single-cell LC period.

4 Energy and Memory States

4.1 Electromagnetic energy

The network stores energy in three components: the cell capacitors, the inductors, and the coupling capacitors between neighbouring cells. It is convenient to define a per-cell energy that assigns half of each coupling capacitor to each adjacent cell. The electromagnetic energy associated with cell k is therefore

$$_k(t) = \frac{q_k(t)^2}{2C} + \frac{L\,i_k(t)^2}{2} + \frac{\big(q_k(t) - q_{k-1}(t)\big)^2}{4C_c} + \frac{\big(q_k(t) - q_{k+1}(t)\big)^2}{4C_c}, \tag{10}$$

with indices understood modulo N. The total energy in the network is

$$_{\rm tot}(t) = \sum_{k=0}^{N-1} {}_k(t). \tag{11}$$

Direct calculation shows that for $R = 0$ the total energy is conserved, whereas for $R > 0$ one obtains

$$\frac{^{\rm tot}}{t} = -R\sum_{k=0}^{N-1} i_k(t)^2 \le 0, \tag{12}$$

so that dissipation is entirely due to ohmic loss in the inductive branches.

In numerical experiments, we track both $_{\rm tot}(t)$ and the spatial distribution of $_k(t)$.

4.2 Energy-level encoding

We interpret the vector of cell energies

$$\mathbf{E}(t) = \big({}_0(t), \ldots, {}_{N-1}(t)\big) \in {}_+^N \tag{13}$$

as an *energy pattern* at time t. Different patterns correspond to different configurations of stored energy.

[Energy memory state] Let $\Omega_j \subset {}_+^N$ be a region of state space and let $T_j > 0$. We say that the network realises an *energy memory state* S_j on the interval $[t_0, t_0 + T_j]$ if:

(a) $\mathbf{E}(t_0) \in \Omega_j$,

(b) $\mathbf{E}(t) \in \Omega_j$ for all $t \in [t_0, t_0 + T_j]$, up to a prescribed tolerance.

The scalar T_j is called the *lifetime* of the memory state.

In practice, we construct Ω_j by specifying constraints on spatial localization and pattern shape. For example, Ω_j may describe states where most of the energy is concentrated in a small subset of cells while other cells remain near zero.

4.3 Localization as memory

A key phenomenon supporting EEM is *energy localization*. Intuitively, localization occurs when a subset of cells carries a significantly larger fraction of the energy than the rest of the ring, and this configuration persists for a long time.

Let $\bar{}_k$ denote the time-averaged energy in cell k over the simulation interval $[0, T]$:

$$\bar{}_k = \frac{1}{T}\int_0^T {}_k(t)\, t. \tag{14}$$

We detect localization by analyzing the profile $\bar{}_k$ across cells: strong peaks in $\bar{}_k$ indicate cells with persistent energy concentration.

[Dominant memory cell] Let $\bar{}_k$ be the time-averaged energy profile. A *dominant memory cell* is any index

$$k^* \in \arg\max_{0\le k\le N-1} \bar{}_k. \tag{15}$$

[Energy lifetime] Let ${}_{\mathrm{tot}}(t) begiven by\ (11). We define the energy\ lifetime \tau$ of a given experiment as the time at which the total energy decays to a specified fraction $\eta \in (0, 1)$ of its initial value:

$${}_{\mathrm{tot}}(\tau) = \eta\, {}_{\mathrm{tot}}(0). \tag{16}$$

Typical choices are $\eta = 1/\mathrm{e}$ or $\eta = 0.5$. The ratio τ/T_0, where T_0 is the single-cell oscillation period, indicates how many oscillations the system can undergo before significant energy loss.

In the simulations, we often observe one or two dominant memory cells, even though the system is fully symmetric apart from initial conditions.

5 Spectral and Modal Analysis

To better understand the origin of the observed localization, we perform a simple modal analysis in the idealised lossless case $R = 0$. Substituting the ansatz

$$q_k(t) = \Re\Big\{ Q_m\, e^{(\omega_m t - k\theta_m)} \Big\}, \qquad \theta_m = \frac{2\pi m}{N}, \quad m = 0, \dots, N-1, \tag{17}$$

into the dimensionless equation (9) with $\gamma = 0$ yields

$$-\omega_m^2 Q_m + Q_m + \kappa\big(2Q_m - Q_m e^{\theta_m} - Q_m e^{-\theta_m}\big) = 0. \tag{18}$$

Simplifying, we obtain the discrete dispersion relation

$$\omega_m^2 = 1 + 2\kappa\big(1 - \cos\theta_m\big), \tag{19}$$

which relates the mode frequency ω_m to the wavenumber θ_m.

In the presence of small damping $\gamma > 0$, standard perturbation arguments show that the eigenfrequencies become complex,

$$\tilde{\omega}_m \approx \omega_m - \frac{\gamma}{2}, \tag{20}$$

so that each mode decays exponentially with rate $\gamma/2$. The coupling parameter κ controls the spectral bandwidth and group velocities, and therefore the rate at which energy can spread around the ring.

While the present system is linear and spatially uniform, localized structures can emerge dynamically due to interference among modes and the specific initial excitation. In more general settings, introducing spatial variations in L_k, C_k, or $C_{c,k}$, or adding weak nonlinearity, can further stabilise localized modes [9, 10].

6 Numerical Method

6.1 Parameter choices

Unless otherwise stated, we use the following base parameters in physical units:

$$N = 16, \quad L = 10^{-3}\,\mathrm{H}, \quad C = 10^{-6}\,\mathrm{F}, \quad C_c = 10^{-6}\,\mathrm{F}, \quad R = 10^{-3}\,\Omega. \tag{21}$$

The corresponding single-cell resonant frequency is

$$\omega_0 = \frac{1}{\sqrt{LC}}, \qquad T_0 = \frac{2\pi}{\omega_0}, \tag{22}$$

and simulations are run over a time horizon of $T = 0.05\,\mathrm{s}$ with 6000 equally spaced samples.

Initial conditions are chosen as follows:

- All currents are zero at $t = 0$: $i_k(0) = 0$.
- A localized energy injection is applied at cell $k = 0$ via a non-zero initial charge:

$$q_0(0) = Q_0, \qquad q_k(0) = 0 \text{ for } k \neq 0, \tag{23}$$

with $Q_0 = 4 \times 10^{-6}\,\mathrm{C}$.

6.2 Time integration

We solve the ODE system using a standard explicit Runge–Kutta scheme of order 5 with embedded error control (as implemented in `solve_ivp` in PYTHON/SciPy). The tolerances are set to

$$\mathrm{rtol} = 10^{-9}, \qquad \mathrm{atol} = 10^{-12}, \tag{24}$$

which are sufficient to ensure that numerical dissipation is negligible compared to physical dissipation from R. We have verified that further tightening these tolerances does not change the results at the scale of the figures presented. A reference implementation of the simulation code (`eem_simulation.py`) and figure-generation scripts accompanies this work and is made available in an online repository (URL omitted here for review).

6.3 Diagnostic quantities

For each simulation we record:

- the total energy trajectory $_{\mathrm{tot}}(t)$;
- the per-cell energy trajectories $_k(t)$;
- the time-averaged profile $\bar{}_k$ defined in (14);
- the dominant memory cell index k^*;
- the energy lifetime τ for a chosen threshold η.

We visualize the results via:

(a) a plot of total energy vs. time;
(b) a space–time heatmap of $_k(t)$;
(c) a spatial plot of $\bar{}_k$ with the memory cell highlighted.

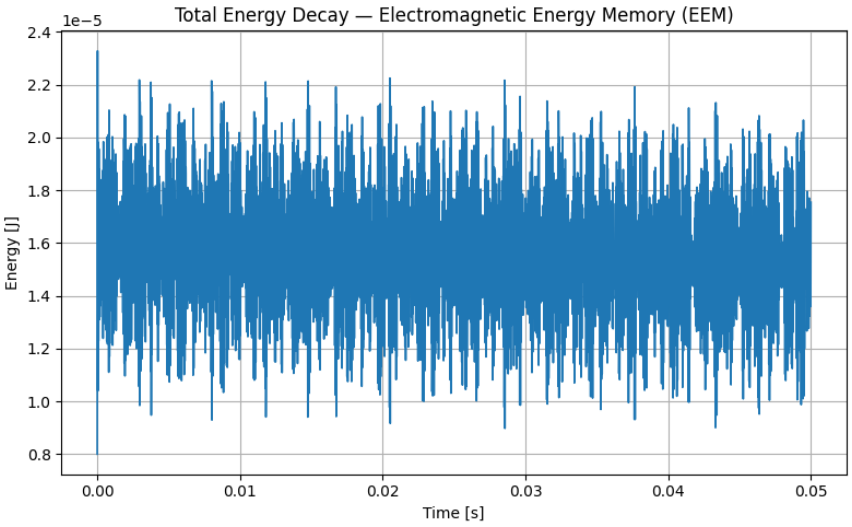

Figure 1: Total electromagnetic energy $_{\text{tot}}(t)$ of the LC ring over the simulation horizon. The envelope decays slowly due to resistive losses, while internal oscillations remain prominent.

7 Results

7.1 Total energy evolution

Figure 1 shows a representative trajectory of the total network energy $_{\text{tot}}(t)$ for the parameter set (21). Despite the presence of ohmic losses, the energy decays slowly over the full simulation window. The trajectory exhibits rich oscillatory behaviour superimposed on a slowly decreasing envelope, indicating that the network operates in a *quasi-conservative* regime where resonant interactions dominate over dissipation on short timescales.

7.2 Space–time energy distribution

Figure 2 depicts the space–time map of per-cell energies $_k(t)$. Time runs along the horizontal axis, while the vertical axis indexes the cells $k = 0, \ldots, N-1$. Colour intensity corresponds to energy magnitude.

A striking feature is the emergence of a persistent horizontal band near cell index $k \approx 8$. Although the initial energy injection occurred exclusively at cell $k = 0$, a second region of elevated energy appears around $k = 8$ and remains visible throughout the simulation. This indicates that the network dynamics and coupling structure promote the formation of a *secondary localized mode*.

7.3 Energy localization profile and memory cells

To quantify localization, we compute the time-averaged energy profile $\bar{}_k$ according to (14) and apply a mild Gaussian smoothing. The resulting profile is shown in Figure 3. Two prominent peaks are visible: a primary peak at cell $k = 0$, corresponding to the injection site, and a secondary peak around cell $k = 8$. The automatically detected dominant memory cell is typically the larger of these peaks, depending on the exact parameters.

The coexistence of multiple localized peaks suggests that EEM networks can support more than one memory state simultaneously, opening the possibility of multi-state or multi-level energy encoding.

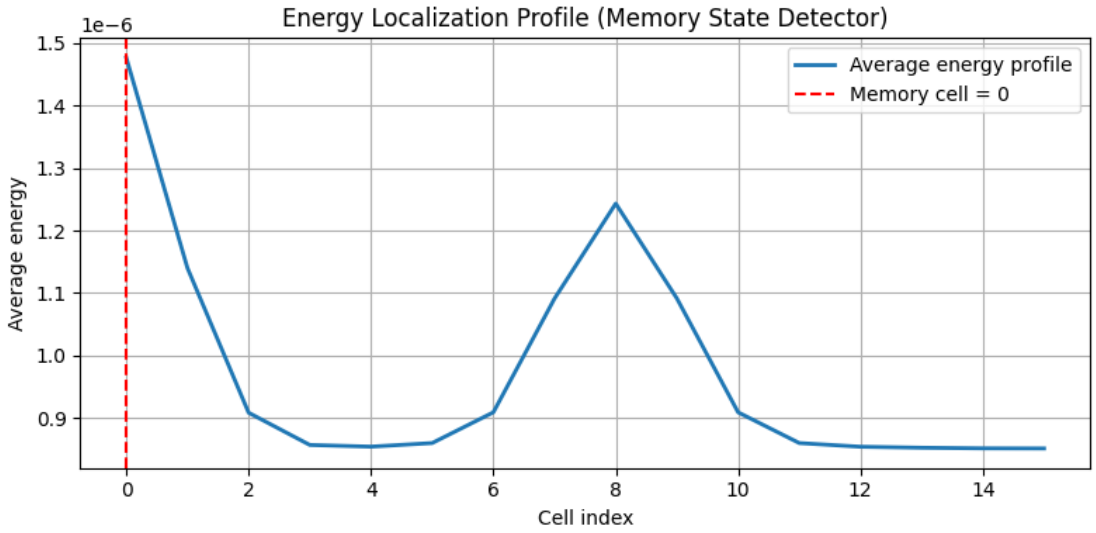

Figure 2: Space–time map of per-cell energy $_k(t)$ for the LC ring. A persistent localized band around cell index $k \approx 8$ indicates the formation of a stable energy memory state, despite energy being injected only at cell $k = 0$.

8 Engineering Limits and Efficiency

The preceding sections establish that EEM networks can, in principle, support long-lived electromagnetic memory states. In this section we provide a first quantitative discussion of energetic limits, quality factors, and parameter sensitivity.

8.1 Upper-bound energy and field constraints

For a single cell, the maximum storable energy is limited by constraints on voltage, current, and material breakdown. Assuming bounds $V_{\max}$ on the capacitor voltage and $I_{\max}$ on the inductor current, a simple upper bound on the cell energy is

$$_{k,\max} \leq \frac{1}{2} C V_{\max}^2 + \frac{1}{2} L I_{\max}^2 + \frac{1}{4C_c} \left(2V_{\max}\right)^2, \tag{25}$$

where the last term corresponds to the worst-case configuration in which the charge difference $|q_k - q_{k\pm1}|$ reaches its maximum value consistent with the same voltage bound. The network-level energy bound is then

$$_{\max} \leq N \, _{k,\max}, \tag{26}$$

up to additional constraints arising from mutual consistency of charges and voltages.

A more refined analysis would incorporate electric-field limits in the dielectric materials, geometric capacitance models, and magnetic saturation in inductive components. Nevertheless, (25) already shows that, at fixed L, C, C_c, the energy density of EEM devices can in principle be increased by pushing materials towards higher breakdown fields, as in advanced capacitor and SMES technologies [3, 4].

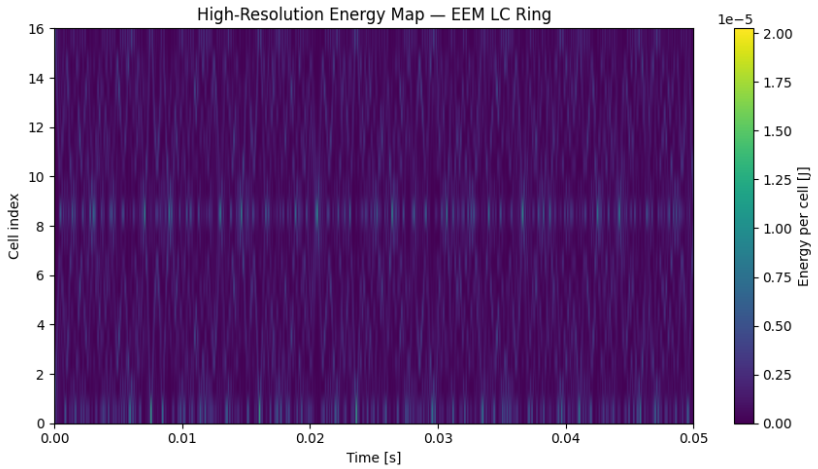

Figure 3: Time-averaged energy localization profile $\bar{}_k$ across the ring. The peaks indicate cells that maintain elevated energy over long timescales and can be interpreted as electromagnetic memory cells.

8.2 Quality factor and retention efficiency

For a single damped LC cell with small series resistance R, the quality factor is

$$Q = \frac{\omega_0 L}{R} = \frac{1}{R}\sqrt{\frac{L}{C}}. \tag{27}$$

In the underdamped regime, the energy decays approximately as

$$(t) \approx (0)\, \exp\!\left(-\frac{\omega_0}{Q}\, t\right), \tag{28}$$

so that the 1/e lifetime is

$$\tau \approx \frac{Q}{\omega_0}. \tag{29}$$

In the coupled network, different normal modes experience slightly different effective damping, but (29) remains a useful guideline: high-Q designs directly translate into longer electromagnetic memory lifetimes.

The *retention efficiency* over a storage interval T_{store} can be defined as

$$\eta_{\text{ret}} = \frac{\text{tot}(T_{\text{store}})}{\text{tot}(0)} \approx \exp\!\left(-\frac{\omega_0}{Q}\, T_{\text{store}}\right), \tag{30}$$

with the approximation becoming increasingly accurate in the high-Q regime. For fixed T_{store}, this relation makes explicit the trade-off between component quality, operating frequency, and acceptable energy loss.

8.3 Sensitivity to network parameters

The parameters L, C, C_c, R play distinct roles:

- Increasing C at fixed $V_{\max}$ and geometry raises the maximum energy but lowers ω_0, potentially increasing τ at fixed Q.

Table 1: Qualitative comparison of EEM with representative energy-storage technologies.

Technology	Cycle life	Response time	Energy density
Li-ion battery	Medium–high	Milliseconds–seconds	High
Supercapacitor	Very high	Sub-millisecond	Medium
SMES	Very high	Sub-millisecond	Medium
Mechanical flywheel	High	Milliseconds	Medium
EEM (this work)	Potentially very high*	Sub-microsecond (RF regime)	Geometry- and material-limited

*In idealised models, the number of charge/discharge cycles is not intrinsically limited by chemical degradation, but by material fatigue, breakdown, and parasitic effects.

- Decreasing R directly increases Q and improves η_{ret}, but may require higher-purity conductors or superconducting materials.
- The coupling capacitance C_c controls both the spectral bandwidth via (19) and the strength of spatial correlations. Too strong coupling (κ large) tends to delocalize energy, while too weak coupling suppresses the formation of secondary memory cells.

A systematic sensitivity analysis, e.g. via parameter sweeps or adjoint-based optimisation, is a natural direction for future work aimed at designing application-specific EEM networks.

9 Comparative Perspective within the Energy-Storage Landscape

EEM does not aim to replace electrochemical technologies outright, but to occupy a distinct niche in the broader energy-storage landscape. Table 1 summarises, at a qualitative level, how EEM compares to several established technologies.

Two points are worth emphasising:

(a) EEM is naturally suited to regimes where *ultra-fast response*, *extreme cycle life*, and *tight integration with analog or RF circuitry* are more important than bulk energy density.

(b) EEM suggests that some functions currently assigned to digital memory (SRAM, DRAM) might, in specialised contexts, be mapped to energy localization patterns in resonant networks, blurring the boundary between *storage* and *computation*.

A full techno-economic comparison would require detailed designs, material choices, and fabrication strategies, which lie beyond the scope of this initial conceptual study.

10 Discussion

The numerical experiments demonstrate that even a simple LC ring with realistic resistive losses can exhibit:

- long-lived energy storage distributed across the network;
- emergent spatial localization not trivially predicted by the initial conditions;
- stable memory cells where energy remains elevated over many oscillation periods.

From an energy-storage perspective, these results show that purely electromagnetic structures can, in principle, maintain distinguishable states over technologically relevant timescales. While the absolute storage capacity of the present model is modest, the concept scales with network size, component values, and possible three-dimensional realizations, and may be especially attractive in regimes where ultra-fast response and extremely high cycle life are required.

From an information-theoretic viewpoint, the mapping

$$\text{initial excitation pattern} \longmapsto \text{long-term energy localization pattern}$$

acts as a form of analog memory. Different excitation configurations may lead to distinct, robust localization profiles, suggesting that networks can be designed to implement energy-based logic or computation.

It is important to emphasise that the present model is *linear* and spatially uniform. The observed localization therefore arises from constructive and destructive interference among extended normal modes, rather than from disorder or strong nonlinearity. As such, the resulting memory states are not topologically protected and can be sensitive to parameter variations and coupling to external circuitry. One promising direction for future work is to combine the EEM framework with deliberately engineered inhomogeneities or weak nonlinear elements, in order to stabilise localized modes and enhance their robustness in the spirit of discrete breathers and topological edge states [9, 10, 11].

Several questions remain open:

(a) How do non-uniform parameters $(L_k, C_k, R_k, C_{c,k})$ affect memory formation and stability?
(b) Can graph-theoretic and topological tools be used to design networks with protected energy modes?
(c) What are the ultimate limits on lifetime and energy density given realistic materials and fabrication constraints?
(d) How can such networks be interfaced with conventional power electronics and control systems?

Addressing these questions will require a combination of circuit theory, numerical optimisation, and experimental prototyping.

11 Conclusion

We have introduced Electromagnetic Energy Memory (EEM) as a resonant, network-based framework for non-chemical energy storage. By modelling a ring of coupled LC cells with resistive loss, we derived the governing equations, defined energy-level encoding, and carried out high-precision simulations. The results show that the network supports long-lived, spatially localized energy modes that can be interpreted as electromagnetic memory states.

Although this work is exploratory and idealised, it establishes a concrete mathematical and computational basis for further investigation. Future research will extend the model to more general network topologies, incorporate material constraints, and explore practical device architectures. If successful, EEM could complement electrochemical storage in regimes requiring fast response, extremely high cycle life, and tight integration with resonant power electronics and analog information processing.

Code Availability

All simulation code, figure-generation scripts, and supplementary materials for this study are openly available at the following GitHub repository:
https://github.com/mohamedorhan/Electromagnetic-Energy-Memory-EEM-.git

This repository contains the full Python implementation of the EEM model, numerical experiments, and the LaTeX source of the paper.

Acknowledgements

The author thanks the broader scientific community for the foundational work on circuit theory, resonant networks, and energy storage that makes this exploration possible.

References

[1] J. B. Goodenough and K.-S. Park, "The Li-ion rechargeable battery: A perspective," *J. Am. Chem. Soc.*, vol. 135, pp. 1167–1176, 2013.

[2] H. Chen, T. Nguyen, A. Martin, G. Luo, and F. Blaabjerg, "Electrical energy storage systems: A critical review," *Prog. Nat. Sci.*, vol. 19, pp. 291–312, 2009.

[3] B. Dunn, H. Kamath, and J. M. Tarascon, "Electrical energy storage for the grid: A battery of choices," *Science*, vol. 334, no. 6058, pp. 928–935, 2011.

[4] X. Li, D. H. Fletcher, and P. F. Blythe, "Superconducting magnetic energy storage systems for power grid applications," *Renew. Sustain. Energy Rev.*, vol. 99, pp. 14–27, 2019.

[5] M. Noori, M. Karimi, S. Tatari, and O. Davoudi, "A review of energy storage systems in microgrids," *Sustain. Cities Soc.*, vol. 28, pp. 473–484, 2016.

[6] D. M. Pozar, *Microwave Engineering*, 4th ed. Wiley, 2011.

[7] J. D. Joannopoulos, S. G. Johnson, J. N. Winn, and R. D. Meade, *Photonic Crystals: Molding the Flow of Light*, 2nd ed. Princeton Univ. Press, 2008.

[8] M. J. Ablowitz, *Nonlinear Dispersive Waves: Asymptotic Analysis and Solitons*. Cambridge Univ. Press, 2011.

[9] S. Flach and C. R. Willis, "Discrete breathers," *Phys. Rep.*, vol. 295, pp. 181–264, 1998.

[10] D. K. Campbell, S. Flach, and Y. S. Kivshar, "Localization in nonlinear lattices," *Phys. Today*, vol. 57, no. 1, pp. 43–49, 2004.

[11] A. E. Miroshnichenko, S. Flach, and Y. S. Kivshar, "Fano resonances in nanoscale structures," *Rev. Mod. Phys.*, vol. 82, pp. 2257–2298, 2010.